

Graphene-based biosensor using transport propertiesR. Chowdhury,^{*} S. Adhikari,[†] P. Rees, and S. P. Wilks
Swansea University, Singleton Park, Swansea SA2 8PP, UK

F. Scarpa

University of Bristol, Bristol BS8 1TR, UK

(Received 6 June 2010; revised manuscript received 7 October 2010; published 3 January 2011)

The potential of graphene nanoribbons (GNR's) as molecular-scale sensors is investigated by calculating the electronic properties of the ribbon and the organic molecule ensemble. The organic molecule is assumed to be absorbed at the edge of a zigzag GNR. These nanostructures are described using a single-band tight-binding Hamiltonian. Their transport spectrum and density of states are calculated using the nonequilibrium Green's function formalism. The results show a significant suppression of the density of states (DOS), with a distinct response for the molecule. This may be promising for the prospect of GNR-based single-molecule sensors that might depend on the DOS (e.g., devices that respond to changes in either conductance or electroluminescence). Further, we have investigated the effect of doping on the transport properties of the system. The substitutional boron and nitrogen atoms are located at the center and edge of GNR's. These dopant elements have significant influence on the transport characteristics of the system, particularly doping at the GNR edge.

DOI: [10.1103/PhysRevB.83.045401](https://doi.org/10.1103/PhysRevB.83.045401)

PACS number(s): 73.22.-f, 73.40.-c

I. INTRODUCTION

Carbon nanotubes (CNT's) have been shown to exhibit significant changes in electronic transport phenomenon due to the presence of absorbed biomolecules.¹⁻⁵ Previous experimental work demonstrating the possibility of using these properties for biosensing applications^{3,4} was performed using nonmetallic CNT's in a field-effect transistor (FET) configuration.⁴ The gate of the FET can be either a metallic back gate or a liquid gate. The back-gated configuration is usually complicated to fabricate, whereas precise controlling of the gate potential is required for liquid-gated devices. However, the detailed mechanism of the interaction is not yet fully understood. Several suggestions have been proposed including electrostatic gating liquid gating case⁴ and electron donation by the detected species.¹

Growing research interest in the application of carbon nanostructure emerged in 2004, led by the experimental discovery of the stable form of graphene.⁶⁻⁸ Graphene is made up of a single layer of carbon atoms packed into a two-dimensional honeycomb lattice. It has attracted tremendous attention in both its two-dimensional and one-dimensional forms, the latter being obtained by patterning the layer into a strip or ribbon.⁹ Scanning probe microscopy of graphene ribbons¹⁰ revealed bright stripes along its edges, suggesting a large density of states at the edge near the Fermi level. The electronic properties of graphene nanoribbons (GNR's)^{11,12} defined by their quasi-one-dimensional electronic confinement and the shape of the ribbon ends,¹³ indicates remarkable applications in graphene-based devices.⁸ GNR's have similarities in many properties of CNT's.¹⁴ However, due to their planar structure, some of the properties seem to be easier to manipulate than CNT's.¹⁵

As for the case of nanotubes, electron transport properties^{16,17} and conductance¹⁸ are expected to be found in graphene structures.^{19,20} In particular, different quantization rules have been predicted for pure GNR's with zigzag

(ZGNR's)²¹ and armchair^{20,22} (AGNR's) edge shaped. Edge states present in zigzag ribbons provide a single channel for electron conduction which is not the case for the armchair configuration. The nature and robustness of these states near the zigzag edges of ZGNR's, for different edge shapes and chemical edge modifications, have been extensively discussed before.²³

In this paper we study the effect of organic molecule adsorption on the transport of single-layer GNR's in a two-probe configuration. In particular, ZGNR's with a quasi-one-dimensional organic fragment are considered here. We choose linear polyaromatic hydrocarbons such as anthracene (see Fig. 1). Understanding their interaction with GNR's will help to understand how full organic or biofragments or proteins (which are too complex to be presently simulated by the state-of-the-art *ab initio* techniques used here) interact with ZGNR's. These molecules could be useful to simulate the effects on the electronic transport of ZGNR's for the development of graphene-based sensor devices. Further, we investigate the effect of doping²⁴ on the transport properties of the system. The substitutional boron and nitrogen atoms are located at the center and edge of GNR's (see Fig. 2). These dopant elements have a significant influence on the transport characteristics of the system, particularly doping at the GNR edge.

II. MODELING AND SIMULATION

The electronic structures and geometry relaxations of the ribbon and the hybrid system of a ribbon with an attached organic molecule are calculated by using density-functional-theory (DFT)-based nonequilibrium Greens function (NEGF) formalism within the TRANSIESTA^{25,26} framework, which is implemented in the ATOMISTIX TOOLKIT (ATK) package (version 2008.02).^{25,27} In our transport calculations, the exchange-correlation potential is described by the local density approximation (LDA).^{26,28} The Troullier-Martins nonlocal

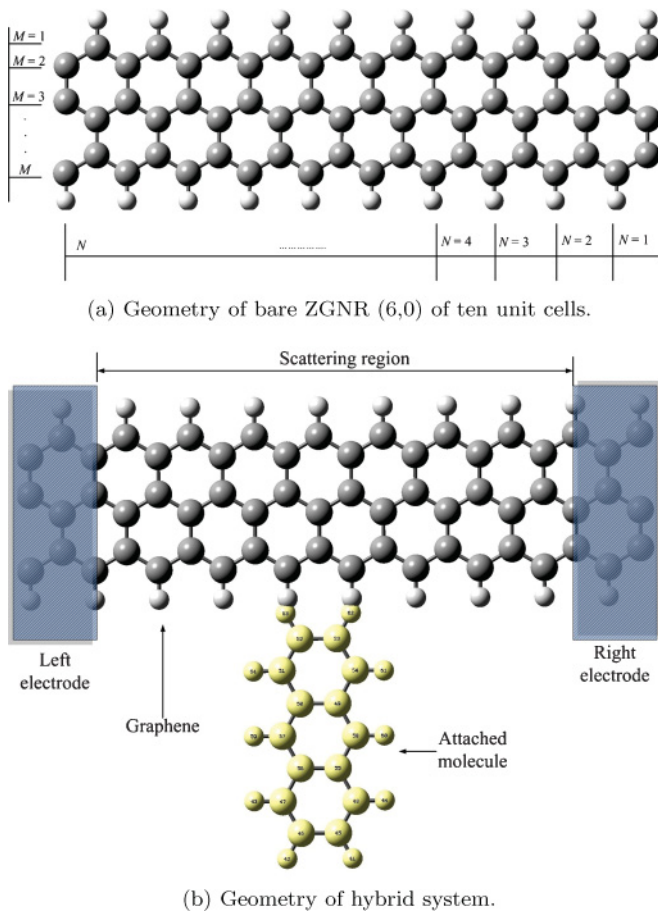


FIG. 1. (Color online) (a) Geometric configuration of bare ZGNR. N denotes the number of repetition unit cells along the length and M denotes the number of atoms along the width. Increasing N and M increases the length and width of ZGNR, respectively. A similar procedure is adopted for the system of ZGNR with an attached organic fragment. (b) Schematic configuration of a two-probe system for a zigzag nanoribbon of ten unit cells in length with attached molecule. The configuration is divided into three regions: left electrode, right electrode, and central scattering region. The attached organic fragment is anthracene ($C_{14}H_{10}$), which is essentially an organic semiconductor. It is a solid polycyclic aromatic hydrocarbon consisting of three fused benzene rings and used as a scintillator for detectors of high-energy photons, electrons, and alpha particles.

pseudopotentials²⁹ are used to model core electrons, and valence electrons are expanded in a SIESTA³⁰ localized basis set. The C-C and C-H bond lengths are set to be 1.42 and 1.1 Å, respectively. All atomic positions are fully relaxed with a force tolerance of 0.001 eV/Å. The system is analyzed with $1 \times 1 \times 300$ uniformly spaced k points (300 k points in the transport direction). We performed a convergence study with respect to k -points sampling. For this purpose, the setup is increased by increasing the k points in the transport direction up to 500; however, there is no change in the transmission spectrum. The self-consistent calculations are performed with a mixing rate set to 0.01 and the convergent criterion for total energy is 10^{-5} eV.

The use of the basis set in the *ab initio* simulations has a significant effect on the results, as demonstrated in.^{31,32}

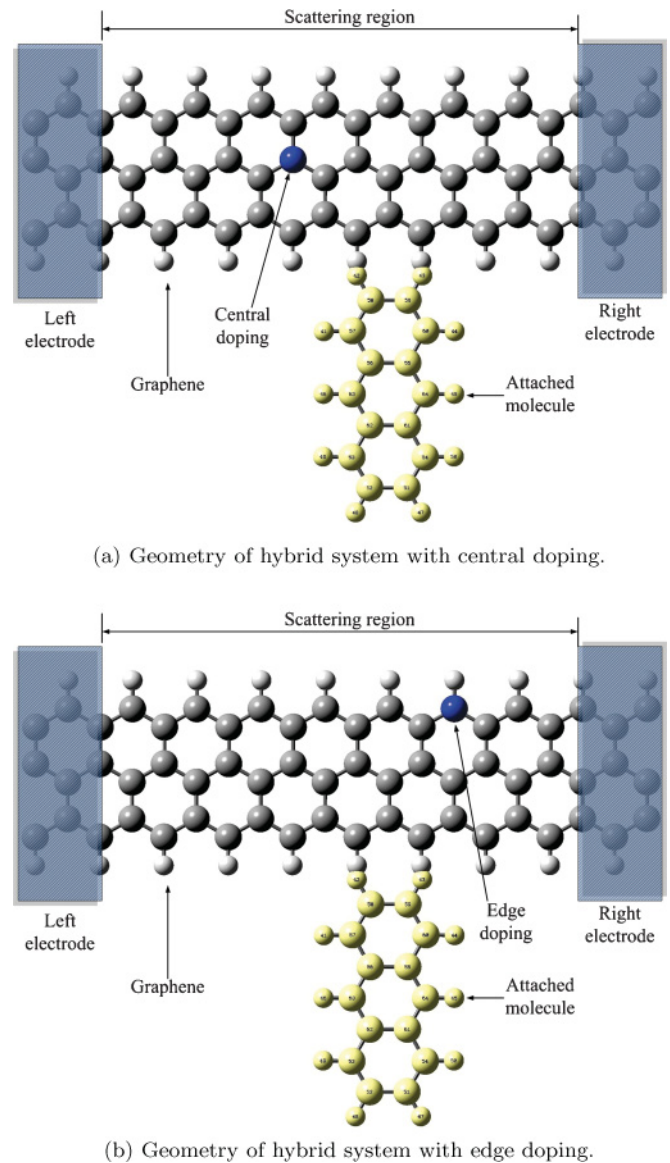


FIG. 2. (Color online) Schematic doped configuration of a two-probe system for a zigzag nanoribbon of ten unit cells in length with attached molecule.

Due to this fact, first we performed bare ZNR's, where we repeated the simulations using the double- ζ and single- ζ basis sets. It was found that the difference between the relative current changes predicted by the double- ζ and the single- ζ basis sets is not significant in the range of the bias used. In our calculations, the single- ζ polarized basis set is used and the mesh cutoff is set to be 150 Ry to save computational time. Moreover, ATK uses periodic boundary conditions in the directions transverse to the transport direction. To assure that no significant interaction occurs between the actual simulation box and its repeated images, as was previously pointed out,⁵ we used the vacuum pad of >10 Å in the x and y directions. It is also noted that vacuum padding is needed to allow electrostatic interactions to decay for systems. The size of the simulation box is increased in the transverse direction till the relative changes in the calculated current are observed as $\sim 1\%$. The transport mechanism²⁷ of the system is studied

using DFT-based NEGF formalism. Using NEGF theory, the transmission coefficients can be obtained as

$$T(E) = \text{tr}(\Upsilon_R G_C \Upsilon_L G_C^\dagger). \quad (1)$$

Here the subscripts C , L , and R are used to denote central scattering, left electrodes, and right electrodes, respectively. G_C and $\Upsilon_{L(R)}$ denote the corresponding Greens functions and imaginary parts of the self-energies, respectively. The current passing through the scattering central region is calculated by the Landauer formula³³

$$I(V) = \frac{2e}{h} \int_{\mu_L}^{\mu_R} [f(E - \mu_L) - f(E - \mu_R)] T(E) dE. \quad (2)$$

Here μ_L and μ_R are the chemical potential of the left and right electrodes, k_B is the Boltzmann constant, T_{temp} is the temperature, $f(E - \mu) = \frac{1}{1 + \exp[\frac{E - \mu}{k_B T_{\text{temp}}}]}$ is the Fermi-Dirac distribution function, and $T(E)$ is the transmission function. The following are program parameters used in the present analyses:

(i) Iteration mixing parameter: Algorithm = Pulay and Diagonal mixing parameter = 0.1;

(ii) Basis set parameters: Type = single- ζ polarized, Radial sampling = 0.001 Bohr, Energy shift = 0.001 Ry, Delta rinn = 0.8, $v_0 = 40.0$ Ry and Split norm = 0.15;

(iii) Iteration control parameters: Tolerance = 10^{-5} , Criterion = Total Energy and Max steps = 500;

(iv) Two probe algorithm parameters: Electrode constraint = Off and Initial density type = Equivalent Bulk;

(v) Energy contour integral parameters: Circle points = 30, Integral lower bound = 3 Ry, Fermi line points = 10, Fermi function poles = 4, Real axis infinitesimal = 0.01 eV and Real axis point density = 0.02 eV;

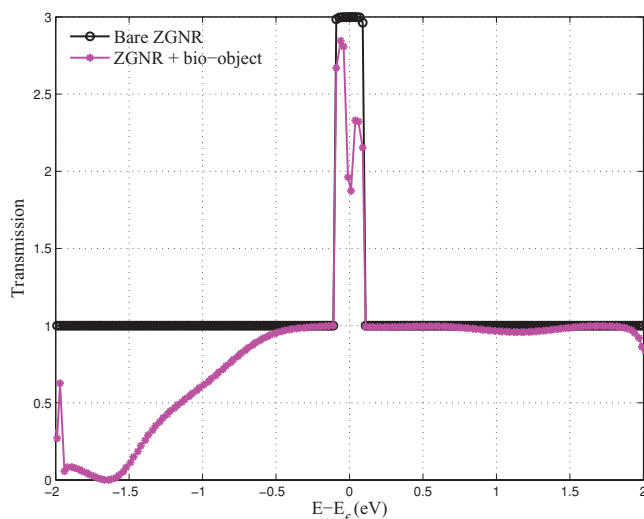
(vi) Two center integral parameters: Cutoff = 2500.0 Ry and Points = 1024.

In the present study, we choose linear polyaromatic hydrocarbons anthracene ($C_{14}H_{10}$) (see Fig. 1), which is essentially a molecular organic semiconductor. It is a solid polycyclic aromatic hydrocarbon consisting of three fused benzene rings and can be used as a scintillator for detectors of high-energy photons, electrons, and alpha particles.

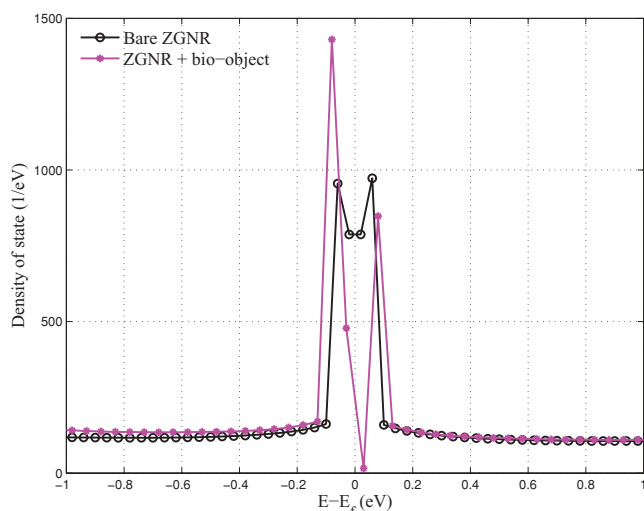
III. RESULTS AND DISCUSSION

A. System of zigzag graphene ribbon

We calculated the system properties of bare ZGNR and ZGNR with attached organic molecules. The band-structure energy (BSE)³⁴ (i.e., the sum of the energies of all states weighted with their respective occupation for bare ZGNR) is found as -1839.04 eV, whereas for ZGNR with attached organic objects, this increases to -2222.71 eV. Figure 3(a) compares the estimated transmission coefficient (T) for the bare ZGNR with organic object attached in ZGNR. All energies are relative to the Fermi energy. It is clear that the ZGNR exhibits metallic behavior: There is no band gap, as observed from other tight-binding calculations.^{9,35,36} The Fermi level ($E_f = 0$) lies at the midgap, and the states contributing to the conduction (contributing states) have a



(a) Transmission for bare ZGNR (6,0) of ten unit cells and the same ZGNR with attached organic-fragment



(b) Density of states

FIG. 3. (Color online) Comparison of (a) the transmission for bare ZGNR (6,0) of ten unit cells and the same ZGNR with attached organic object as a function of energy at equilibrium. The calculation was performed at ambient temperature $T = 300$ K. The BSE for bare ZGNR is found as -1839.04 eV, whereas for ZGNR with attached organic molecule, this increases to -2222.71 eV. At the energy range of about ± 0.2 eV, there is one conducting channel which results in a unit transmission coefficient. However, the transmission drops down about 35% due to the attachment of the organic object at the Fermi level. (b) DOS for the bare (6,0) ZGNR and the same ZGNR with attached polyaromatic hydrocarbons. It can be observed that there is a large reduction of states near to the Fermi level due to the attachment of hydrocarbons. This results in the reduction of the NDR phenomenon of ZGNR.

range of energy of about ± 0.2 eV. A decrease in T in the energies corresponding to the gap states is observed when the polyaromatic hydrocarbon is attached to the bare ZGNR. This may be explained by the hydrocarbon competing with the ZGNR for the states injected from the electrodes. The coupling of ZGNR with the organic object also reduces the gap state, which can be further demonstrated through Fig. 4.

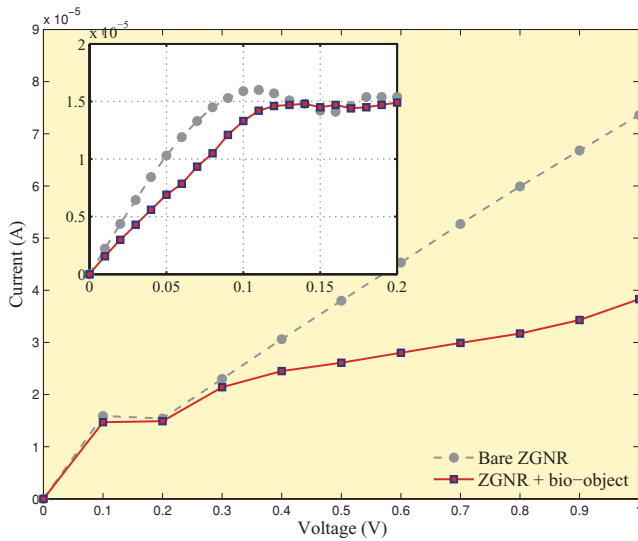


FIG. 4. (Color online) I - V characteristics for the bare ZGNR (6,0) of ten unit cells in length and the same ZGNR with attached polyaromatic hydrocarbons. The inset figures show the NDR of ZGNR and ZGNR with attached organic molecules. The origin of NDR in this system is due to the large reduction in the transmission when the bias exceeds about 0.13 V. It is also found that the attachment of hydrocarbons reduces the NDR of ZGNR. The origin of this reduction can be traced back from the transmission [see Fig. 3(a)] and the DOS [see Fig. 3(b)].

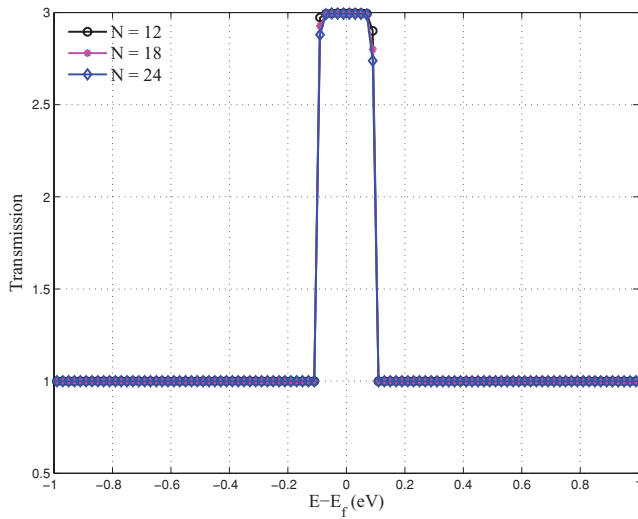
The current (I)-voltage (V) characteristics of the (6,0) ribbon are shown in Fig. 4 for the bare ribbon and for the same ribbon with an attached organic object. It is clear that in both cases the current increases with bias, then virtually saturates until 0.2 V. When V exceeds 0.2, the current starts again to increase with the applied bias. This indicates the onset of a new carrier transport mechanism. It is noticed that the attaching of the aromatic molecule results in a small reduction in current when $V \leq 0.2$, while it has a significant effect for higher bias levels. It induces a larger decrease in the current for $V \geq 0.2$, but also causes a clear increase in the current when V exceeds 0.2. To understand the presented result, we now explain the large transmission coefficients presented in the figures. The transmission probability for a single incoming electron wave is always between 0 and 1. The transmission spectrum, plotted in this study, is not a spectrum of the probability of a single electron being transmitted through the two-probe. It is the sum of the probability of all the single modes being transmitted through the two-probe, so if there, at a given energy, are three block waves called A, B, and C, then the transmission spectrum is the sum of the probability of A, B, and C added together. A similar characteristic for bare graphene was reported in a recent study.³⁷ Now we explain the mechanism of the transport phenomenon for an explanation for the features of the (I - V) characteristics.

When the applied bias is lower than the band gap of the system (note that band gap refers to the electronic structure of the ZGNR) in a scattering region, electrons can move from the left electrode to the right electrode in the free states of the conduction band creating a left-to-right current (LRC). In a similar manner, electrons can move into the free states in the left electrode from the conduction band of the right electrode

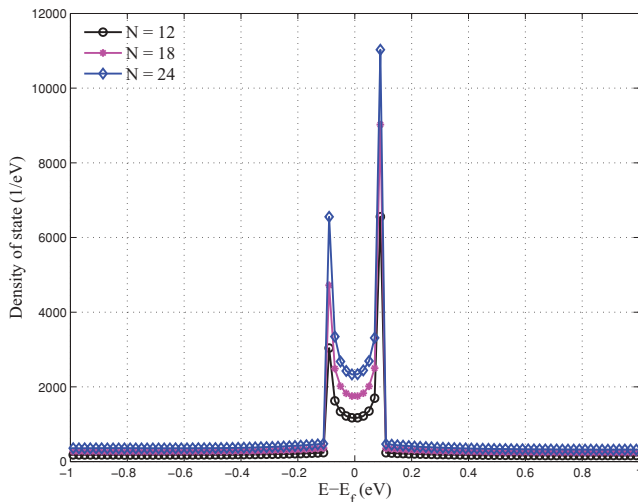
creating a right-to-left current (RLC). However, the current due to the former mechanism will be greater than the latter mechanism. This is caused mainly by the energy barrier. As the bias increases, the energy barrier increases and therefore RLC decreases. Eventually, RLC gets saturated. Electrons in the valence band of the left electrode cannot tunnel to the right electrode until the applied bias is less than the band gap of the system in the scattering region. This is due to the unavailability of states at the corresponding energies on the right electrode. As the applied bias is increased and exceeds the band gap, free states of the right electrode become available and then start contributing to the electrode-electrode tunneling. This mechanism makes a sudden increase in the current when $V \geq 0.3$.

The inset figures of Fig. 4 show the negative differential resistance (NDR) phenomenon^{9,38-40} in the I - V curves of ZGNR and ZGNR with attached organic molecules. To understand the origin of NDR in this system, in Fig. 4 we compare the transmission coefficients at the current peak and valley voltages. We observe NDR in the I - V characteristics as has been previously observed in nanotube and ribbon structures with a zigzag chain configuration.^{9,38-41} The origin of this effect is due to the need for parity conservation of the incoming and outgoing electronic wave functions. It can also be argued that the existence of the negative differential resistance region is due to the gap in the transmission coefficient.⁴¹ As one can see from the figure, there is a large reduction in the transmission when the bias exceeds about 0.13 V. It is also found that the attachment of hydrocarbons reduces the NDR of ZGNR. The origin of this reduction can be traced back from the transmission [see Fig. 3(a)] and the density of states (DOS) [see Fig. 3(b)]. The DOS shown in Fig. 3(b) is integrated over the contributing states energies described previously. The state significantly drops down due to the coupling of hydrocarbon to the ZGNR. Moreover, the calculated charge of bare ZGNR is about $207.96q$ (where q is the electronic charge), compared to a charge of $252.46q$ in the case of ZGNR with attached organic objects. Further study is needed to see the effect of the attachment of an aromatic molecule with a semiconducting ribbon (e.g., AGNR), which is the focus of future work.

To study the variation of the DOS and transport properties with the length and width of the ZGNR system, we have calculated the DOS and transport by varying the lengths and widths of the ribbon. Figures 5 and 6 present the variation of different properties for different lengths and widths. The strong dependence of the transmission and DOS on the ribbon can be observed from the presented figures. This may be explained by the fact that the band gap of the bare graphene ribbon decreases with increasing ribbon width.³⁷ In a recent CNT-based sensor study,⁵ it was reported that the current of the bare tube is larger (at the same bias) for larger-radius tubes due to their smaller band gap. The current is calculated as the integral of the transmission. Therefore, following the similar argument made for the CNT-based sensor, the current in the ribbon increases with ribbon width, which, in turn, demonstrates the increasing of the transmission with increasing ribbon width. Furthermore, the strong rise in the transmission upon increasing the widths of the ribbons were reported in very recent studies.^{37,42,43} Next, we consider the effect of the concentration of adsorbed



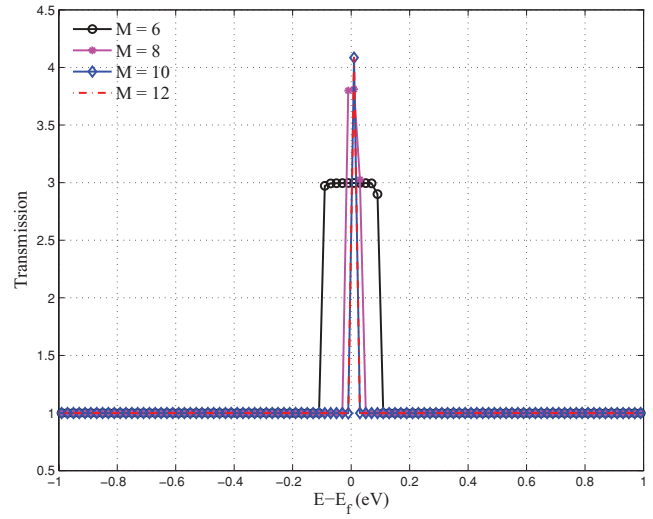
(a) Transmission spectrum



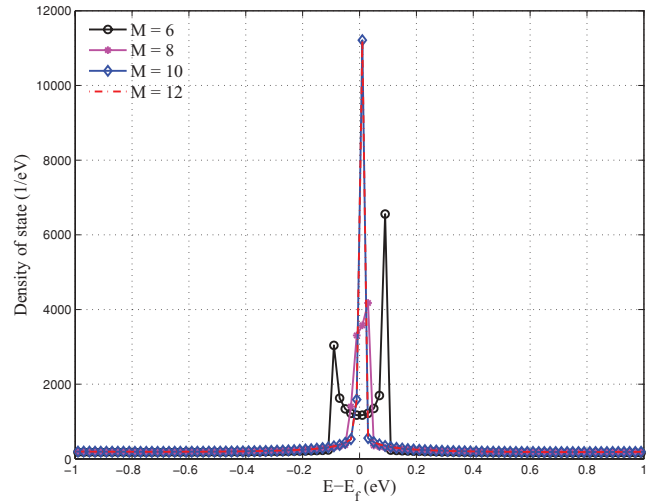
(b) Density of states

FIG. 5. (Color online) Comparison of (a) the transmission for ZGNR, as a function of energy at equilibrium and (b) DOS. The width of the ribbon [see Fig. 1(a)] is kept as $M = 6$, while the length is varying 4 [e.g., N is increasing as in Fig. 1(a)].

molecules on the conductance. Figure 7 presents the variation of conductance and the DOS on absorbed molecules. Note that the first three molecules are attached sequentially in one side edge of the graphene and the other three molecules are attached sequentially at the other edge of the graphene. It can be observed that, for the first three molecules, there is very little change in transmission. However, due to the attachment of molecules at the other edges, transmission/conductance drops down significantly. This can be explained as follows. In the structure there are two conductance paths for electronic transfer on either side of the ribbon. Due to the absorption of molecules, the local density of electronic states along the conductance path available for conduction decreases. In this study we have considered the first three molecules to be absorbed on one side of the ribbon, while the remaining three are added to the other side. The first three molecules block conduction in one conductance path, however, the other path



(a) Transmission spectrum



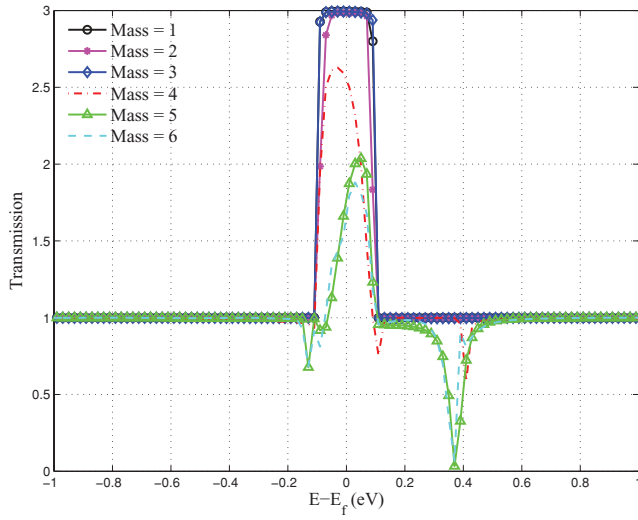
(b) Density of states

FIG. 6. (Color online) Comparison of (a) transmission for ZGNR, as a function of energy at equilibrium and (b) DOS. The length of the ribbon [see Fig. 1(a)] is kept as $N = 12$, while the width is varying [e.g., M is increasing as in Fig. 1(a)].

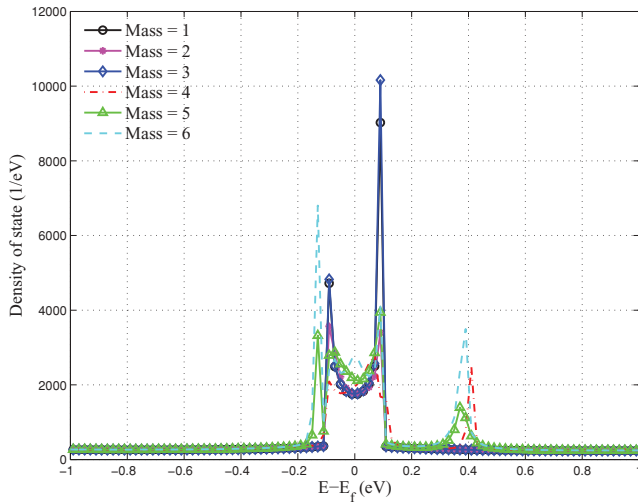
is available for conduction so the transmission is only slightly reduced. When the molecules attach to the second conductance path, waves are blocked in this conductance path. This causes the transmission to reduce significantly. Due to this fact, we observed a strikingly different behavior in this graphene-based sensor study. Clearly, when acting as a sensor, in general, there is no control over to which edge the molecules might attach. For this reason, we studied attached molecules on both edges of the graphene ribbon.

B. Effect of doping

In this section we examine the effect of doping on ZGNR with attached organic objects. The BSE for boron doped at the center is found as -2183.06 eV, whereas for doping at the edge, it is about -2192.50 eV. Clearly there is no significant difference in band energies. However, compared



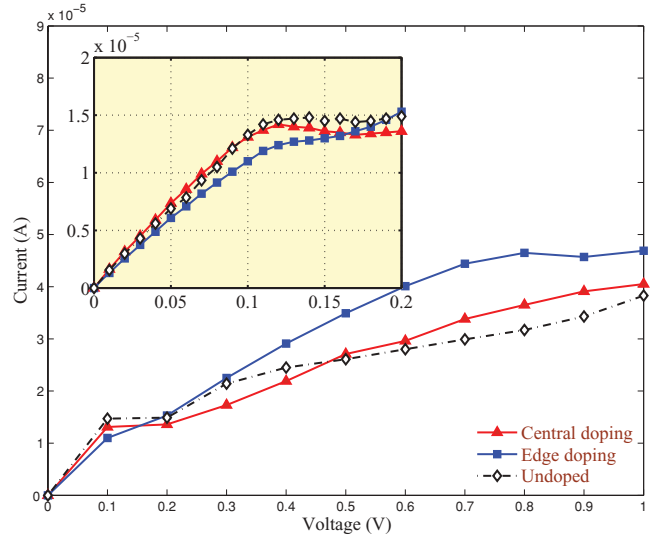
(a) Transmission spectrum



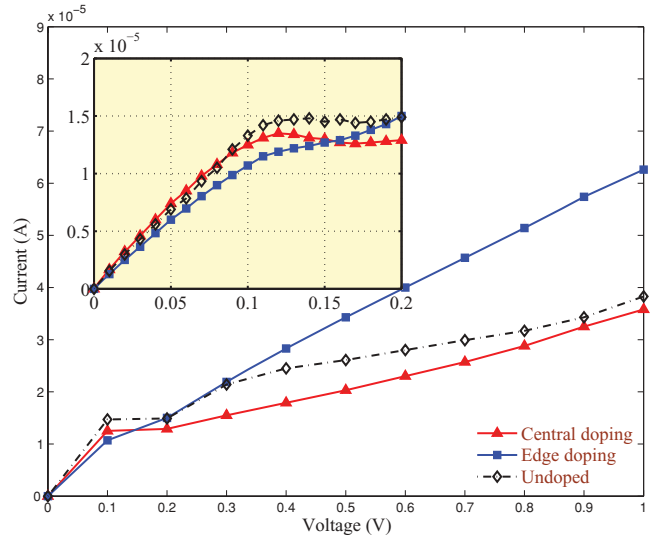
(b) Density of states

FIG. 7. (Color online) (a) Effect of concentration of adsorbed molecules on the conductance. The attached molecules are arranged along length [$M = 18$ as in Fig. 1(a)]. In the figure, Mass = 6 denotes that six molecules are attached to the ribbon. The calculated total energies for different configurations are as follows: $-20\,378.48$ eV, $-22\,044.70$ eV, $-23\,723.85$ eV, $-25\,356.74$ eV, $-26\,928.01$ eV, and $-28\,528.93$ eV for Mass = 1,2,3,4,5, and 6, respectively. Note that the first three molecules are attached sequentially in one edge of the graphene and the other three molecules are attached sequentially at the other edge of the graphene. It can be observed that, for the first three molecules, there is very little change in transmission. However, due to the attachment of molecules at the other edges, transmission/conductance drops down significantly. (b) Density of states.

to the undoped system the band energy of the doped system reduces to about 30 eV. Similarly, for nitrogen doping at the center, the BSE is found as -2264.61 eV, whereas for doping at the edge, it is about -2250.89 eV. This clearly demonstrates that nitrogen doping increases the band energy by about 42 eV. Figure 8 shows the I - V characteristics of the (6,0) ribbon with an attached organic fragment, both boron and nitrogen doping. We observe the same trend of the current



(a) Doping with Boron



(b) Doping with Nitrogen

FIG. 8. (Color online) I - V characteristics (a) for boron and (b) nitrogen doped at the center and edge of ZGNR with attached polyaromatic hydrocarbon. The inset figures show the NDR of ZGNR with attached organic molecules along with the corresponding doped system. We notice that the effect of the edge doping has a strictly increasing pattern, whereas for central doping the current is virtually bias independent from $V = 0.1$ to $V = 0.2$ and NDR phenomenon can be observed. It can also be observed that current transmission due to edge doping is much greater compared to the undoped system at $V \geq 0.2$. In contrast, central doping makes a reduction in current transmission. However, the small applied voltage transmission of current in a doped system is always smaller than the undoped system.

with increasing bias as mentioned previously. We notice that the effect of the edge doping has a strictly increasing pattern, whereas the central doping current is virtually bias independent from $V = 0.1$ to $V = 0.2$ and NDR phenomenon can be observed. It can also be observed that current transmission due to edge doping is much greater compared to the undoped system at $V \geq 0.2$. In contrast, central doping makes a

reduction in current transmission. For small applied voltage, however, the transmission of current in the doped system is always lower than the undoped system. We also noticed that the doping of nitrogen at the ribbon edge is significantly higher than others. This may be attributed to the fact that edge nitrogen is able to inject more states into the system. The calculated charge of central and edge doping due to boron is about $251.59q$ and $251.48q$, respectively, whereas due to nitrogen doping it is about $253.39q$ and $253.44q$, respectively.

IV. CONCLUSION

In this work we demonstrated that GNR shows a clear change in conductance in response to the attachment of an aromatic molecule. We also studied the effect of doping on the energy states as well as the transport properties of GNR with attached organic objects. There exist different transport mechanisms depending on the applied bias. These type of structures seem to be useful to describe, qualitatively, the effects on the transport properties of ZGNR when organic

molecules are attached to the ribbon edges. The energy states and transmission of the ZGNR suggests that ZGNR can be used as a spectrograph sensor device. Additionally, the significant effect of doping on these quasi-one-dimensional systems can be observed in the transmission spectrum. Based on these results, one may propose an extended and more detailed study of these nanostructures acting as nanosensor devices. An interesting task would be to investigate the effect of a large number of molecules randomly distributed along the ribbon edges on transport properties of these hybrid systems. A systematic analysis following this line may be useful to determine the type and concentration of foreign entities which could be detected with these kinds of structures.

ACKNOWLEDGMENTS

RC acknowledges the support of the Royal Society through the award of a Newton International Fellowship. SA gratefully acknowledges the support of the Leverhulme Trust for the award of the Philip Leverhulme Prize.

*r.chowdhury@swansea.ac.uk

†s.adhikari@swansea.ac.uk

¹G. Gruner, *Anal. Bioanal. Chem.* **384**, 322 (2006).

²K. Balasubramanian and M. Burghard, *Anal. Bioanal. Chem.* **385**, 452 (2006).

³J. Wang, *Electroanalysis* **17**, 7 (2005).

⁴I. Heller, A. M. Janssens, J. Mannik, E. D. Minot, S. G. Lemay, and C. Dekker, *Nano Lett.* **8**, 591 (2008).

⁵G. B. Abadir, K. Walus, and D. L. Pulfrey, *Nanotechnology* **21**, 015202 (2010).

⁶M. Ezawa, *Phys. Rev. B* **73**, 045432 (2006).

⁷A. Hirsch, *Angew. Chem., Int. Ed.* **48**, 6594 (2009).

⁸H. Santos, L. Chico, and L. Brey, *Phys. Rev. Lett.* **103**, 086801 (2009).

⁹V. N. Do and P. Dollfus, *J. Appl. Phys.* **107**, 063705 (2010).

¹⁰B. Biel, X. Blase, F. Triozon, and S. Roche, *Phys. Rev. Lett.* **102**, 096803 (2009).

¹¹Y. Li, Z. Zhou, P. Shen, and Z. Chen, *J. Phys. Chem. C* **113**, 15043 (2009).

¹²E.-J. Kan, Z. Li, J. Yang, and J. G. Hou, *J. Am. Chem. Soc.* **130**, 4224 (2008).

¹³L. Rosales, M. Pacheco, Z. Barticevic, A. Latgé, and P. A. Orellana, *Nanotechnology* **19**, 065402 (2008).

¹⁴D. V. Kosynkin, A. L. Higginbotham, A. Sinitskii, J. R. Lomeda, A. Dimiev, B. K. Price, and J. M. Tour, *Nature (London)* **458**, 872 (2009).

¹⁵E. Prodan and R. Car, *Phys. Rev. B* **80**, 035124 (2009).

¹⁶Y.-Y. Zhang, J.-P. Hu, X. C. Xie, and W. M. Liu, *Physica B-Condensed Matter* **404**, 2259 (2009).

¹⁷N. M. R. Peres, *J. Phys.: Condens. Matter* **21**, 323201 (2009).

¹⁸X. Du, I. Skachko, A. Barker, and E. Y. Andrei, *Nature Nanotechnology* **3**, 491 (2008).

¹⁹J. A. Rogers, *Nature Nanotechnology* **3**, 254 (2008).

²⁰H. B. Heersche, P. Jarillo-Herrero, J. B. Oostinga, L. M. K. Vandersypen, and A. F. Morpurgo, *Nature (London)* **446**, 56 (2007).

²¹J. Park, H. Yang, K. S. Park, and E.-K. Lee, *J. Chem. Phys.* **130**, 214103 (2009).

²²S. K. Maiti, *Solid State Commun.* **149**, 973 (2009).

²³K. Nakada, M. Fujita, G. Dresselhaus, and M. Dresselhaus, *Phys. Rev. B* **54**, 17954 (1996).

²⁴T. B. Martins, R. H. Miwa, A. J. R. da Silva, and A. Fazzio, *Phys. Rev. Lett.* **98**, 196803 (2007).

²⁵M. Brandbyge, J. Mozos, P. Ordejon, J. Taylor, and K. Stokbro, *Phys. Rev. B* **65**, 165401 (2002).

²⁶A. Grigoriev, N. V. Skorodumova, S. I. Simak, G. Wendin, B. Johansson, and R. Ahuja, *Phys. Rev. Lett.* **97**, 236807 (2006).

²⁷J. Taylor, H. Guo, and J. Wang, *Phys. Rev. B* **63**, 245407 (2001).

²⁸J. Perdew and A. Zunger, *Phys. Rev. B* **23**, 5048 (1981).

²⁹N. Troullier and J. Martins, *Phys. Rev. B* **43**, 1993 (1991).

³⁰J. Soler, E. Artacho, J. Gale, A. Garcia, J. Junquera, P. Ordejon, and D. Sanchez-Portal, *J. Phys.: Condens. Matter* **14**, 2745 (2002).

³¹G. B. Abadir, K. Walus, and D. L. Pulfrey, *Appl. Phys. Lett.* **94**, 176101 (2009).

³²D. Michalska, L. J. Schaad, P. Carsky, B. A. Hess, and C. S. Ewig, *J. Comput. Chem.* **9**, 495 (1988).

³³Y. Meir and N. S. Wingreen, *Phys. Rev. Lett.* **68**, 2512 (1992).

³⁴J. Taylor, H. Guo, and J. Wang, *Phys. Rev. B* **63**, 245407 (2001).

³⁵S. Reich, J. Maultzsch, C. Thomsen, and P. Ordejon, *Phys. Rev. B* **66**, 035412 (2002).

³⁶B. Gharekhanlou, M. Alavi, and S. Khorasani, *Semicond. Sci. Technol.* **23**, 075026 (2008).

³⁷U. Treske, F. Ortmann, B. Oetzel, K. Hannewald, and F. Bechstedt, *Phys. Status Solidi A* **207**, 304 (2010).

³⁸H. Cheraghchi and K. Esfarjani, *Phys. Rev. B* **78**, 085123 (2008).

³⁹H. Ren, Q.-X. Li, Y. Luo, and J. Yang, *Appl. Phys. Lett.* **94**, 173110 (2009).

⁴⁰H. Cheraghchi and H. Esmailzade, *Nanotechnology* **21**, 205306 (2010).

⁴¹D. Dragoman and M. Dragoman, *Appl. Phys. Lett.* **90**, 143111 (2007).

⁴²D. Basu, M. J. Gilbert, L. F. Register, S. K. Banerjee, and A. H. MacDonald, *Appl. Phys. Lett.* **92**, 042114 (2008).

⁴³F. Schwier, *Nature Nanotechnology* **5**, 487 (2010).